



## Intrinsic defect migration in Be<sub>12</sub>Ti

M.L. Jackson<sup>a,b</sup>, P.A. Burr<sup>c,\*</sup>, R.W. Grimes<sup>a</sup>

<sup>a</sup> Centre for Nuclear Engineering, Department of Materials, Imperial College London, SW7 2AZ, UK

<sup>b</sup> Culham Centre for Fusion Energy, Culham Science Centre, Abingdon, Oxfordshire, OX14 3DB, UK

<sup>c</sup> School of Mechanical and Manufacturing Engineering, University of New South Wales, Sydney, NSW, 2052, Australia

### ABSTRACT

Be<sub>12</sub>Ti is a leading candidate neutron-multiplier material for fusion breeder blankets; yet the evolution of the crystal defects under irradiation is poorly understood. Here, the migration of intrinsic defects in tetragonal Be<sub>12</sub>Ti was predicted using atomic scale computer simulation. Transport of titanium and beryllium through the interstitial, interstitialcy and vacancy-mediated models was considered, along with the migration of divacancy clusters, previously identified as important to the defect chemistry of Be<sub>12</sub>Ti. It was found that titanium defects exhibit much higher migration energies than beryllium for most migration pathways, leading to a dramatic difference in the self-diffusivity of the two species. Both beryllium vacancy and interstitial diffusion is close to isotropic with vacancy transport exhibiting the highest self-diffusion coefficient. Migration of beryllium di-vacancies is also isotropic with activation energy equal to that of isolated vacancies. The titanium interstitial exhibits significantly lower migration energy than its vacancy (1.00 eV and 6.75 eV respectively), with both mechanisms strongly anisotropic: the activation energy for [001] migration is at least 5 eV lower than other directions. Even the more exotic mixed titanium beryllium vacancy migration exhibits a much higher migration energy than [001] titanium interstitial transport. The framework used for predicting defect transport kinetics, including vacancy-mediated, interstitial and interstitialcy mechanisms, can be applied to any complex-structured intermetallic compound.

### 1. Introduction

Beryllium rich intermetallics, most notably Be<sub>12</sub>Ti, Be<sub>12</sub>V and Be<sub>13</sub>Zr are being considered as replacements for pure beryllium in nuclear fusion applications [1–7]. It is anticipated that they offer reduced tritium retention [8–13], improved irradiation tolerance [10,14] and general survivability in the fusion environment [14,15], compared to pure beryllium [10]; while maintaining similar neutronic properties for use as a neutron multiplier [16], as well as a low average atomic mass and vapour pressure. These properties are key for first wall material applications [17].

Beryllium metal has long been used in the nuclear industry [18–20], but beryllides, and in particular Be<sub>12</sub>Ti, have only relatively recently been considered for fusion applications [3,16,21]. Several experimental studies have evaluated irradiation effects in Be<sub>12</sub>Ti [14,22,23], generally corroborating the expected improvements in tritium retention and radiation tolerance compared to pure beryllium [12]. While this is promising, the environment in a fusion reactor such as Iter or Demo cannot at present be adequately replicated experimentally, and as such, to qualify Be<sub>12</sub>Ti for use in these reactors, a combined approach of experiments and modelling is desirable.

The defect chemistry of these materials, which ultimately informs the mechanisms of radiation damage and microstructural degradation,

has only recently been probed using atomistic modelling approaches. Work by Allouche et al. [24] on the isomorphic Be<sub>12</sub>W structure used DFT to simulate the interactions of vacancies and hydrogen. They found that the intermetallic exhibits a significantly greater beryllium vacancy formation enthalpy compared to pure beryllium. Fujii et al. [25] used similar methodology to calculate the solution energy of hydrogen at Be<sub>12</sub>Ti interstitial sites to be between 0.1 and 0.7 eV. In addition, the accommodation, migration and interaction of H and He with intrinsic defects has been simulated by Zhu et al. [26,27]. It was found that H and He can be accommodated interstitially with solution energy 0.50 and 4.03 eV, but both bind strongly to Be and Ti vacancies respectively with solution energy –0.26 and 0.94 eV respectively. Further, up to 10 and 4 H atoms can be accommodated on a Ti and Be vacancy. Bachurin and Vladimirov [28] considered the accommodation of H in further detail, finding an interstitial solution energy of 0.43–1.38 eV and binding energies with Be vacancies as strong as –0.3 eV.

In our previous work [29], intrinsic defect accommodation was investigated in four Be<sub>12</sub>M beryllides ( $M = \text{Ti, V, Mo, W}$ ) using density functional theory (DFT). It was found that for Be<sub>12</sub>Ti, Schottky and beryllium Frenkel disorder are the dominant processes for accommodating radiation damage, resulting in (relatively) high concentrations of V<sub>Be</sub>, Be<sub>i</sub> and V<sub>Ti</sub> (although other defects may become significant during damage cascades). Further, it was found that some small defect clusters

\* Corresponding author.

E-mail address: [p.burr@unsw.edu.au](mailto:p.burr@unsw.edu.au) (P.A. Burr).

<https://doi.org/10.1016/j.intermet.2020.106937>

Received 30 April 2020; Received in revised form 11 August 2020; Accepted 13 August 2020

Available online 17 October 2020

0966-9795/© 2020 Elsevier Ltd. All rights reserved.

exhibit negative binding energy (i.e. are stable), particularly  $V_{Be}V_{Be}$ ,  $V_{Be}V_{Ti}$  and  $Ti_{Be}V_{Be}$  (note: in this latter cluster a titanium atom sits in the middle of a Be di-vacancy).

Notably, none of the previous studies considered the transport kinetics of these defects, which is crucial in predicting the evolution of the crystal and the microstructure under irradiation conditions. In this study, diffusion mechanisms are established and migration energies predicted, using DFT based simulations, for those intrinsic defects in  $Be_{12}Ti$  identified in previous work to be most prevalent. The relative migration rates of these species determines how point defects coalesce to form extended defects such as voids and dislocations, and as such aids in our understanding of how radiation damage will evolve in this material.

## 2. Methodology

DFT simulations were carried out using the Perdew, Burke and Ernzerhof scheme of the Generalised Gradient Approximation (GGA) for the exchange-correlation functional [30]. All calculations were performed using the CASTEP code [31], and employed ultra-soft pseudo potentials with a consistent cut-off of 480 eV (converged to  $10^{-3}$  eV. atom $^{-1}$ ). Parameters were chosen to be consistent with those of the previous study [29].

Cells for defect calculations were optimised (without symmetry constraints) in supercells constructed from  $2 \times 2 \times 2$  full  $Be_{12}Ti$  unit cells, containing 208 atoms. A high density of k-points, with spacing of approximately  $0.003 \text{ nm}^{-1}$ , corresponding to k-point grids of  $2 \times 2 \times 4$  for defect calculations, was used for the integration of the Brillouin Zone, following the Monkhost-Pack scheme [32]. As  $Be_{12}Ti$  is metallic, density mixing and Methfessel-Paxton [33] cold smearing of bands were employed with a width of 0.1 eV. Calculations were not spin-polarised. Convergence for all parameters, including the k-point spacing was achieved to at least  $10^{-3}$  eV atom $^{-1}$ . For atomic relaxation in defective cells, the energy convergence criteria for self-consistent calculations was set to  $10^{-7}$  eV, the forces on atoms less than  $0.01 \text{ eV \AA}^{-1}$  and where the cell was relaxed the stress component less than 0.05 GPa.

The formation energy of defects,  $E_f$ , was calculated from the defective and pristine DFT supercells as

$$E_f = E_{defective}^{DFT} - E_{pristine}^{DFT} \pm \sum_i n_i \mu_i \quad (1)$$

where  $\mu_i$  is the chemical potential of the species  $i$  added or removed from the pristine supercell to form the defective supercell, and  $n_i$  is greater than 1 only when defect clusters are considered. The chemical potential of Be and Ti atoms is taken from DFT calculations of the metals in their elemental ground state (hcp-Be and hcp-Ti). The binding energy,  $E_b$ , of defect clusters is calculated from the formation energies as the formation energy of the cluster minus the formation energy of the constituent defects. With this definition, a negative binding energy implies a that the cluster is stable with respect to the dilute defects. Note that the binding energy is also independent on the choice of chemical potential, as these terms cancel out.

Migration barriers were investigated using the transition state search algorithms implemented in CASTEP. First the transition state was identified and optimised using the Linear Synchronous Transit (LST) and Quadratic Synchronous Transit (QST) methodologies [34]. This approach was adopted as it is considerably less computationally expensive than a NEB search, while still accurately predicting the transition energy [34,35]. The full path was obtained using the nudged elastic band (NEB) method [36], with constrained maxima and end-points. A total of nine nodes (including the transition state) between the initial and final configurations were used, employing the same convergence criteria as defect calculations.

The self-diffusion coefficients were calculated using Onsager theory, informed by formation and migration energies from DFT simulations. The Onsager transport coefficient ( $L_{ij}$ ) links the diffusion flux ( $J_i$ ) to the

chemical potentials ( $\mu_i$ ) of species Be and Ti

$$\begin{pmatrix} J_{Be} \\ J_{Ti} \end{pmatrix} = - \begin{pmatrix} L_{BeBe} & L_{BeTi} \\ L_{TiBe} & L_{TiTi} \end{pmatrix} \begin{pmatrix} \nabla \mu_{Be} \\ \nabla \mu_{Ti} \end{pmatrix}$$

However, since Be and Ti vacancies diffuse in separate sublattices, and the vacancies do not readily jump from one sublattice to the other (i. e. the anti-site formation energy is highly unfavourable [29]), we can safely assume that the flux of Be and Ti vacancies are decoupled, that is, the off-diagonal terms  $L_{BeTi}$  and  $L_{TiBe}$  for vacancy-mediated diffusion are zero. We make a further assumption that the flux of interstitials of one species does not significantly affect the flux of vacancies of the other species.

With these simplification, and considering the dilute limit, where the chemical potential of a species is proportional to its concentration, we can relate the Onsager transport coefficient to the diffusion coefficient  $D$  [37] by:

$$D_i = \frac{k_B T \Omega}{c_i} L_{ii}$$

where  $\Omega$  is the volume per atom, and  $c_i$  is the concentration of migrating defects. The equilibrium concentration is determined from the defect formation energy  $E_f$  following the Arrhenius relation:

$$c_i \approx \exp\left(\frac{-E_f}{k_B T}\right)$$

in which the site entropy is implicitly discounted as it is negligible at the high temperatures of interest for diffusion.

The calculations were performed with the aid of the Onsager code by Trinkle [38,39]. The method calculates the Onsager coefficients in the dilute limit by solving a master equation that describes the transitions from one state to another in terms of jump frequencies, similarly to the self-consistent mean field method [40–42]. The method exploits crystal symmetry and is automated for arbitrary crystals. The master equation is informed by the crystal symmetry, the relative formation energies of the different states (atomic configurations) and the migration energy of the individual jumps to connect two states. A jump attempt frequency of 6 THz was used for all jumps, as this is representative of a typical vibrational mode in the material [43]. Compared to the migration energies, which affect the activation energy for diffusion, the attempt frequencies have a marginal effect on the overall diffusivity at the temperatures of interest ( $>900 \text{ K}$ ), provided they are of the correct order of magnitude. When calculating the diffusivity of interstitials and vacancies, all jumps were included in the calculation, irrespective of the associated migration energy or whether they formed part of the lowest energy contiguous pathway for diffusion.

Diffusion was calculated separately for each sublattice and each species. When a species may diffuse through more than one mechanism, the total equilibrium self-diffusion is simply given by [37]:

$$D_i = D_i^1 + D_i^2 + \dots + D_i^n$$

We considered three mechanisms: vacancy, interstitial and interstitialcy. The latter involves a concerted migration of two atoms: an interstitial atom hopping onto a lattice site, and the lattice atom hopping into a new interstitial site. We calculated the interstitialcy diffusion mechanism by treating it as a special case of interstitial migration, as performed previously [44,45]: all concerted jumps were considered as interstitial jumps from starting and ending interstitial sites (with no regards for the intermediate lattice site), but with the migration energy informed by the DFT simulations of the relevant concerted jump. As such, the two atoms involved in a concerted jump appear indistinguishable during the Onsager calculations, and the resulting diffusion coefficients represent self-diffusivity not tracer diffusivity. Onsager calculations of di-vacancy clusters were not performed owing to the increased complexity of the migration process of defect clusters. However, we acknowledge that recent advances in the self-consistent

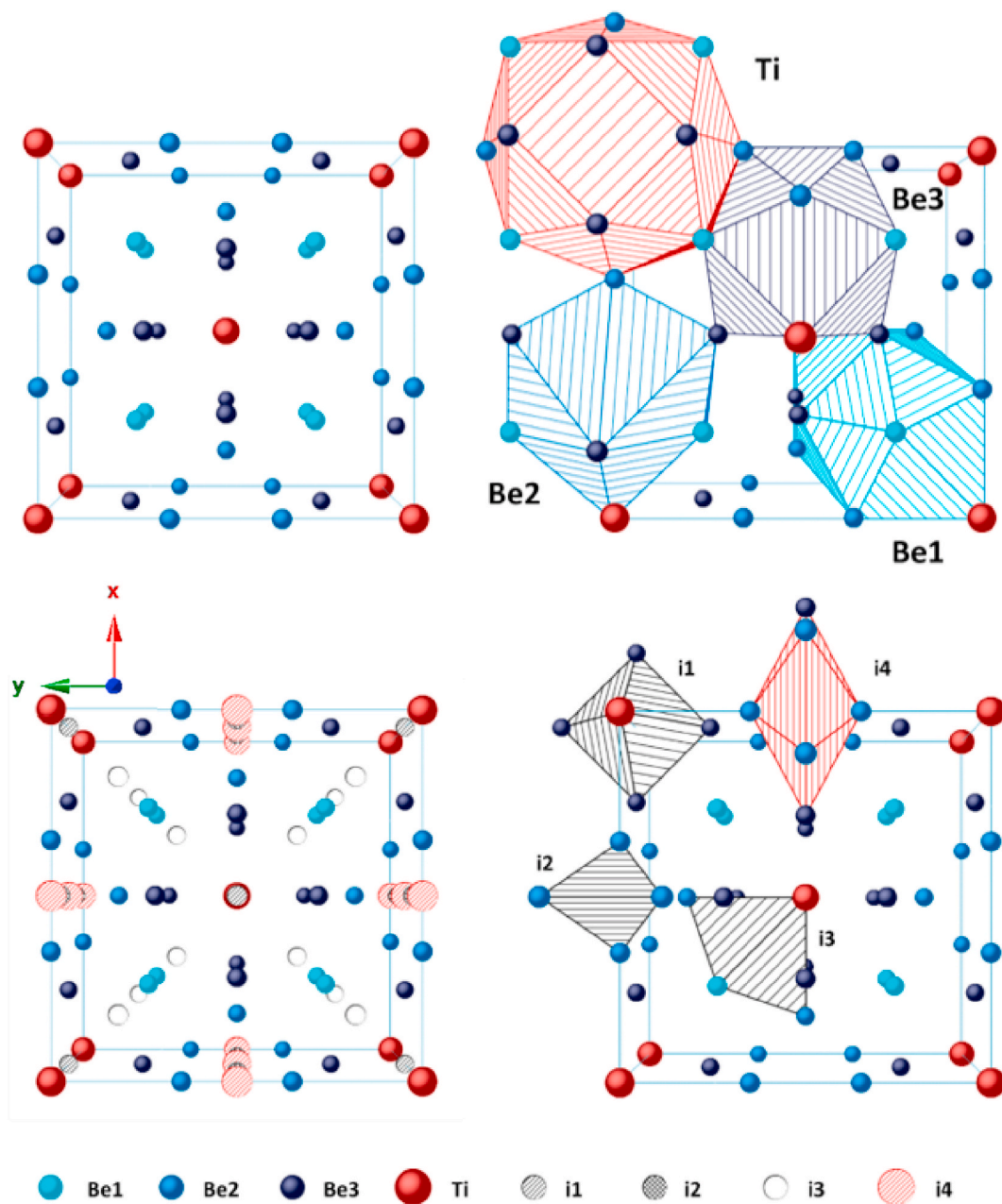


Fig. 1. – Top: crystal structure of  $\text{Be}_{12}\text{Ti}$  [46] with ball model (left) and atomic polyhedra (right). Bottom: interstitial sites shown with patterned balls (left) and polyhedral (right). Reproduced from [29].

mean-field theory approach, implemented in the KineCluE code [42], enable calculations of transport coefficient including clusters. Further work would be required to adapt the method to the specific case  $\text{Be}_{12}\text{Ti}$ , and the results presented here provide the basis for such endeavour.

### 2.1. Crystallography

To provide a framework within which migration of intrinsic defects can be understood, the crystal structure of  $\text{Be}_{12}\text{Ti}$  is depicted in Fig. 1(a) with site polyhedra (b) and interstitial sites (c) with polyhedra (d).  $\text{Be}_{12}\text{Ti}$  has a tetragonal structure with  $I4/mmm$  symmetry [46–48] and lattice parameters  $a = 7.35 \text{ \AA}$  and  $c = 4.19 \text{ \AA}$  (at room temperature) [46]. Our DFT-calculated lattice parameters are in close agreement:  $a = 7.359 \text{ \AA}$  and  $c = 4.164 \text{ \AA}$ , and the agreement improves when thermal expansion is taken into account using the quasi-harmonic approximation, as reported previously [47]. In this structure, beryllium atoms reside on 8f, 8i

Table 1

Calculated formation energies of vacancies and interstitials [29].

Be vacancies	$E_f$ (eV)	Ti vacancies	$E_f$ (eV)
$V_{\text{Be1}}$	1.60	$V_{\text{Ti}}$	4.10
$V_{\text{Be2}}$	1.43		
$V_{\text{Be3}}$	1.53		
Be interstitials	$E_f$ (eV)	Ti interstitials	$E_f$ (eV)
$\text{Be}_{\text{i1}}$	3.23	$\text{Ti}_{\text{i1}}$	5.37
$\text{Be}_{\text{i2}}$	1.86	$\text{Ti}_{\text{i2}}$	5.10
$\text{Be}_{\text{i3}}$	3.96	$\text{Ti}_{\text{i3}}$	7.47
		$\text{Ti}_{\text{i4}}$	4.19

**Table 2**

Binding energies of Be and Ti vacancy pairs with respect to  $V_{Be2}$  and  $V_{Ti}$  (where a negative  $E_b$  means the pair is stable with respect to the dilute defects) [29].

Species	$E_b$ (eV)	Species	$E_b$ (eV)
$V_{Be3}V_{Be3}$ (in plane)	0.41	$V_{Be2}V_{Be1}$	0.26
$V_{Be3}V_{Be3}$ (out of plane)	0.44	$V_{Be1}V_{Be1}$	0.38
$V_{Be2}V_{Be3}$ (in plane)	0.30	$V_{Be1}V_{Be3}$	0.63
$V_{Be2}V_{Be3}$ (out of plane)	0.04	$V_{Ti}V_{Ti}$	0.50
$V_{Be2}V_{Be2}$ (in plane)	0.22	$V_{Ti}V_{Be3}$	-0.04
$V_{Be2}V_{Be2}$ (in plane)	0.35	$V_{Ti}V_{Be2}$	-0.41
$V_{Be2}V_{Be2}$ (out of plane)	-0.04	$V_{Ti}V_{Be1}$	-0.02

**Table 3**

Calculated migration energies of beryllium and titanium vacancies. R is the reactant and P the product. The lowest energy processes from which contiguous pathways can be constructed are identified in bold.

Crystallographic direction/plane	Jump length (Å)	reaction	$E_m$ (eV)		$E_m + E_f$ (eV)
			From R	From P	
anisotropic - [001]	2.08	$V_{Be1} \rightarrow V_{Be1}$	0.76	0.76	2.36
<b>Isotropic</b>	<b>2.13</b>	$V_{Be1} \rightarrow V_{Be3}$	<b>0.61</b>	<b>0.69</b>	<b>2.21</b>
Isotropic	2.24	$V_{Be2} \rightarrow V_{Be2}$	0.91	0.73	2.34
non-percolating (110)	2.21	$V_{Be2} \rightarrow V_{Be2}$	0.50	0.50	1.93
anisotropic - [001]	2.60	$V_{Be2} \rightarrow V_{Be2}$	1.39	1.38	2.82
anisotropic - (110)	3.75	$V_{Be2} \rightarrow V_{Be2}$	4.07	4.07	5.50
anisotropic - (110)	2.34	$V_{Be2} \rightarrow V_{Be3}$	1.19	1.09	2.62
Isotropic	2.29	$V_{Be2} \rightarrow V_{Be3}$	0.94	0.84	2.37
anisotropic - [001]	3.58	$V_{Be3} \rightarrow V_{Be3}$	3.07	3.07	4.60
anisotropic - (110)	2.29	$V_{Be3} \rightarrow V_{Be3}$	1.05	1.05	2.58
<b>anisotropic - [001]</b>	<b>4.16</b>	$V_{Ti} \rightarrow V_{Ti}$	<b>6.75</b>	<b>6.75</b>	<b>10.85</b>

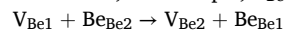
and 8j sites (here referred to as Be1, Be2 and Be3 respectively), and titanium atoms at 2a. Four interstitial sites were identified in prior work at 2b, 4b, 8h and 4c positions, herein referred to as i1, i2, i3 and i4 [29]. All of these sites can accommodate a titanium atom, however beryllium interstitials at the i4 site were observed to relax to i2 sites.

When investigating migration, both the defect migration energy and formation energy contribute to the overall activation energy for migration. In this context, Table 1 presents defect formation energies for the species investigated in this work (relative to their elemental reference states). These were used in previous work [29] to demonstrate that at thermal equilibrium up to 1400 K we expect  $V_{Be}$  and  $V_{Ti}$  species to be available in significantly larger concentrations than  $Ti_i$  and  $V_{Ti}$ . After ballistic collision cascades, the radiation damage was predicted to be accommodated chiefly by  $V_{Be}$ ,  $Be_i$  and  $V_{Ti}$ , while  $Ti_i$  will be present in concentrations that are order of magnitude smaller. Table 2 presents binding energy for divacancies, as reported in [29]. These show that specific pair combinations are stable with respect to isolated species, which offers the possibility transport processes involving two vacancies, as compared to simple single vacancy hopping. Beryllium di-interstitial pairs were not stable except for  $Be_{i4}Be_{i4}$ , which exhibit a small binding energy of -0.10 eV. However, given that  $Be_{i4}$  is not a stable beryllium defect in isolation, and that no other Be di-interstitial cluster may form, it is unlikely that this cluster affects the overall diffusion kinetics of Be interstitials significantly.

### 3. Results and discussion

#### 3.1. Vacancy migration

Migration energies for vacancy migration processes are reported in Table 3 where, for example,  $V_{Be1} \rightarrow V_{Be2}$  is shorthand for:



While the  $V_{Be2} \rightarrow V_{Be2}$  transition exhibits the lowest migration energy of 0.50 eV, alone it does not form a contiguous migration pathway. The lowest energy transition that forms a contiguous pathway is  $V_{Be1} \rightarrow V_{Be3}$  which is isotropic with an  $E_m$  of 0.69 eV. This is followed by the  $V_{Be1} \rightarrow V_{Be1}$  transition in the [001] direction with  $E_m$  0.76 eV. When the formation energy of the defect is considered, in addition to  $E_m$ ,  $V_{Be1} \rightarrow V_{Be3}$  also has the lowest energy for a percolated migration pathway,  $E_f + E_m = 2.21$  eV, followed by  $V_{Be2} \rightarrow V_{Be1}$  and  $V_{Be1} \rightarrow V_{Be1}$  with  $E_f + E_m = 2.34$  and 2.36 eV respectively. As both the  $V_{Be1} \rightarrow V_{Be3}$

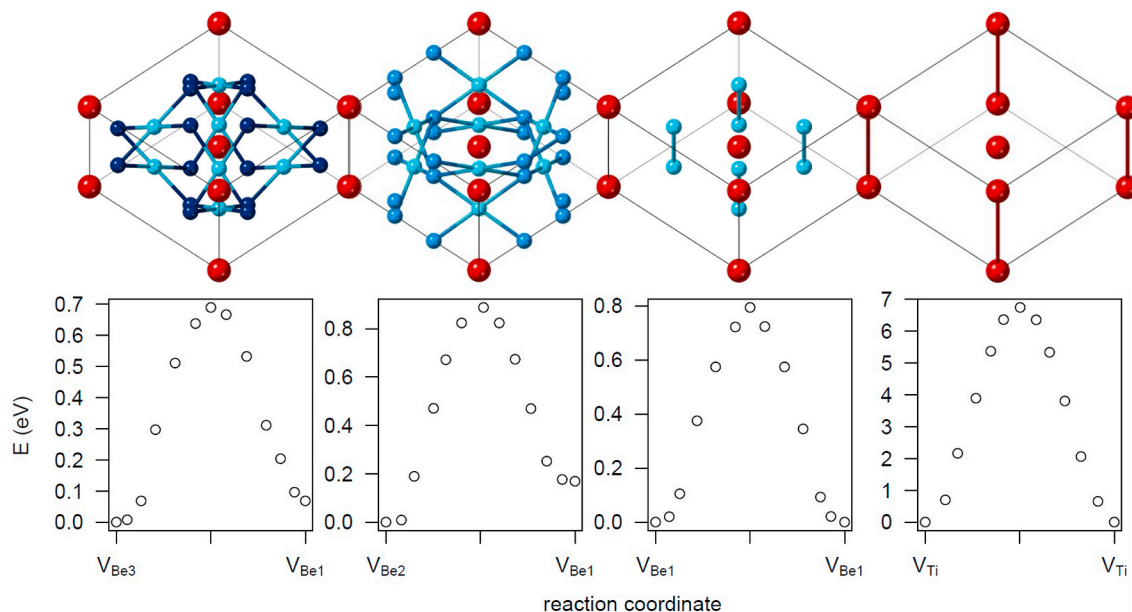


**Fig. 2.** Lowest energy NEB migration pathways for beryllium and titanium vacancy migration processes.

**Table 4**

Beryllium and titanium interstitial migration energies between interstitial sites, as calculated using the LSTQST methodology. R is reactant, P is product. Lowest energy contiguous pathways for isotropic and anisotropic diffusion are identified in bold.

	Jump length (Å)	Reaction	$E_m$ (eV)		$E_f + E_m$ (eV)
			From R	From P	
anisotropic - [001]	2.646	$Be_{i3} \rightarrow Be_{i1}$	0.56	1.29	4.52
<b>anisotropic - [001]</b>	<b>2.082</b>	<b><math>Be_{i2} \rightarrow Be_{i2}</math></b>	<b>1.19</b>	<b>1.19</b>	<b>3.05</b>
anisotropic - (001)	2.311	$Be_{i3} \rightarrow Be_{i3}$	0.47	0.47	4.43
Isotropic	2.924	$Be_{i3} \rightarrow Be_{i2}$	0.42	2.52	4.38
anisotropic - (001)	3.571	$Be_{i3} \rightarrow Be_{i1}$	5.10	5.84	9.06
Isotropic	3.825	$Be_{i1} \rightarrow Be_{i2}$	0.34	1.72	3.57
Isotropic	3.825	$Be_{i2} \rightarrow Be_{Be2}$	1.37	0.02	3.23
		$Be_{Be2} \rightarrow Be_{i1}$			
<b>anisotropic - [001]</b>	<b>2.082</b>	<b><math>Be_{i2} \rightarrow Be_{Be2}</math></b>	<b>1.45</b>	<b>1.45</b>	<b>3.31</b>
		<b><math>Be_{Be2} \rightarrow Be_{i2}</math></b>			
Isotropic	2.966	$Be_{i2} \rightarrow Be_{Be2}$	2.22	0.13	4.08
		$Be_{Be2} \rightarrow Be_{i3}$			
anisotropic - (001)	2.844	$Be_{i3} \rightarrow Be_{Be1}$	0.20	0.20	4.16
		$Be_{Be1} \rightarrow Be_{i3}$			
<b>anisotropic - [001]</b>	<b>1.040</b>	<b><math>Ti_{i2} \rightarrow Ti_{i4}</math></b>	<b>0.15</b>	<b>1.04</b>	<b>5.19</b>
anisotropic - (001)	2.311	$Ti_{i3} \rightarrow Ti_{i3}$	3.28	3.28	10.75
anisotropic - [001]	2.646	$Ti_{i3} \rightarrow Ti_{i1}$	5.10	7.20	12.57
Isotropic	2.924	$Ti_{i2} \rightarrow Ti_{i3}$	6.92	4.55	12.02
anisotropic - (001)	2.777	$Ti_{i3} \rightarrow Ti_{i4}$	4.73	8.04	12.20

and  $V_{Be2} \rightarrow V_{Be1}$  pathways allow diffusion in 3 dimensions and are similar in  $E_f + E_m$ , it can be concluded that diffusion will be broadly isotropic and proceed along all three beryllium sublattices. It is interesting to note that for  $V_{Be}$ ,  $E_m$  correlates strongly and positively with jump length – this is discussed in greater detail below.

In contrast to beryllium transport, titanium vacancy ( $V_{Ti}$ ) migration has a significantly higher activation energy of 6.75 eV, which proceeds in the [001] direction. Furthermore, there are no viable isotropic diffusion pathways for titanium vacancies.

The full NEB energy/reaction coordinate pathways are presented in Fig. 2 for the three lowest energy beryllium vacancy migration pathways and the titanium vacancy migration pathway. The NEB pathways follow typical energy transition pathways for vacancy migration: reaction coordinates for each NEB replica represent the fractional distance the

replica sits along the computed NEB pathway. Based on the LST-QST and NEB results, it is predicted that beryllium vacancy diffusion is isotropic with modest activation energy, while titanium vacancy diffusion is strongly anisotropic to the [001] direction and has high activation energy.

### 3.2. Interstitial and interstitial migration

The migration of interstitials was also considered, since these are predicted to be a dominant defect following radiation damage [17]. Transitions of beryllium and titanium interstitials between nearest neighbour interstitial sites and via displacing an atom from its lattice site (i.e. the interstitialcy mechanism) were investigated using the LST-QST methodology. The numerical results are presented in Table 4 and NEB pathways for the lowest energy transitions shown in Fig. 3.

The lowest energy beryllium interstitial transition is an interstitialcy mechanism with an i3 interstitial atom displacing a lattice beryllium to an adjacent i3 site with activation energy 0.20 eV. The  $Be_{i3}$  species, however, has a formation energy of 3.96 eV, 2.10 eV higher than  $Be_{i2}$ , and furthermore this transition does not, by itself, form a contiguous pathway, thus transport through  $Be_{i2}Ti$  cannot be achieved by this mechanism alone. However, this jump may contribute to the overall diffusivity by connecting other interstitial or interstitialcy jumps. The lowest energy contiguous pathway is an interstitial mechanism via i2 sites in the [001] direction, with activation energy 1.19 eV (the i2 sites also have the lowest interstitial formation energy, see Table 1). Isotropic beryllium interstitial migration may occur via a combination of the interstitial  $i2 \rightarrow i2$  hop and the interstitialcy  $i2 \rightarrow Be2$ ,  $Be2 \rightarrow i2$  hops, the latter of which has rate determining migration energy of 1.45 eV. Although the  $i1 \rightarrow i3$  transition has lower migration energy than this (1.29 eV), the higher formation energy of the i1 and i3 sites make this transition less relevant under thermal equilibrium conditions.

Titanium interstitial migration exhibits an activation energy of 1.00 eV for the  $i4 \rightarrow i2$  transition, which provides a contiguous pathway but only in the [001] direction. This is significantly lower than the lowest energy isotropic transition, which is  $i2 \rightarrow i3$  with migration energy 6.92 eV. As such, while beryllium interstitial migration is predicted to be weakly anisotropic, titanium interstitial migration strongly anisotropic favouring [001].

### 3.3. Diffusivity

Combining all 26 jumps reported above, it is possible to create a holistic picture of diffusion processes of dilute intrinsic defects in  $Be_{12}Ti$  (i.e. that do not involve clusters of defects). The correlation between  $E_m$  and jump length ( $x$ ) is explored for beryllium defects in Fig. 4. Migration

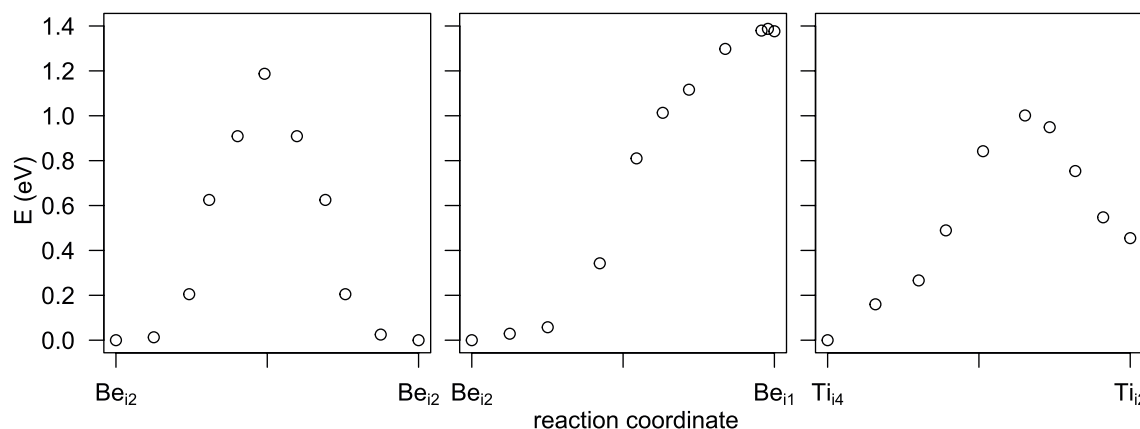


**Fig. 3.** Lowest migration energy pathways for a) beryllium interstitial migration in [001] b) beryllium interstitialcy migration c) titanium interstitial migration in [001]. Together a) and b) form a contiguous pathway for isotropic migration.

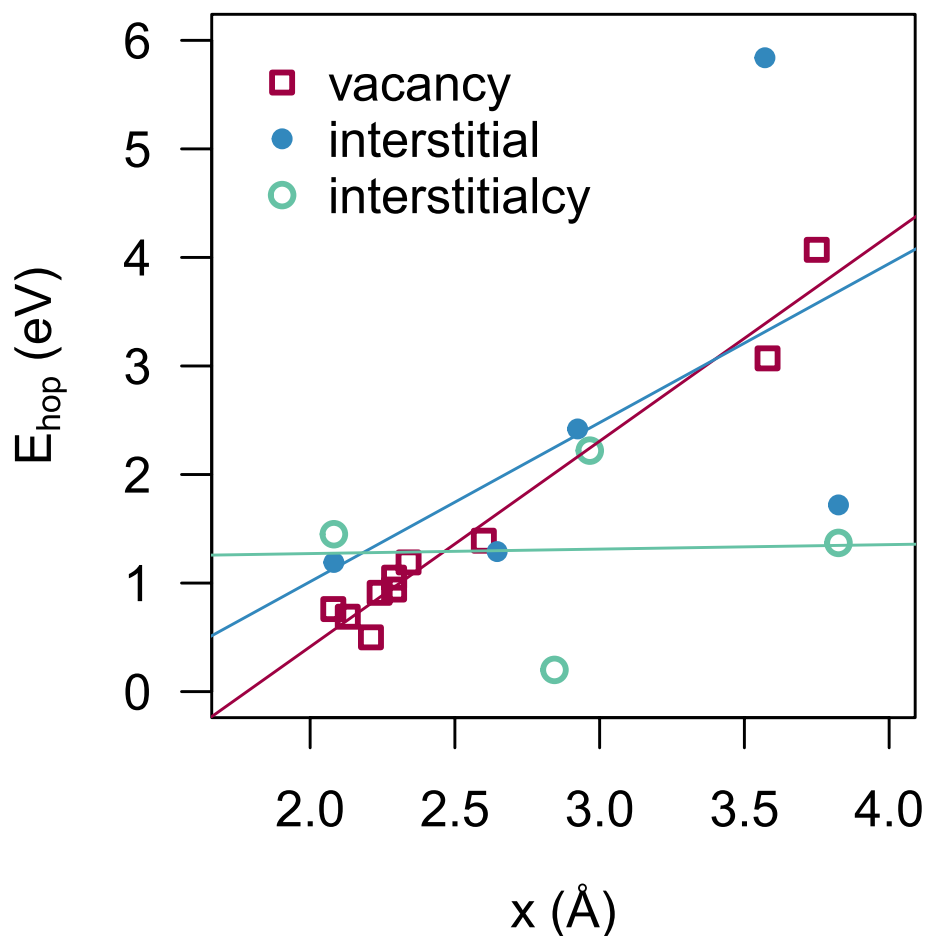


Fig. 4. Relationship between hopping distance and  $E_m$  for beryllium vacancies and interstitials (the latter by both a simple and interstitialcy mechanisms).

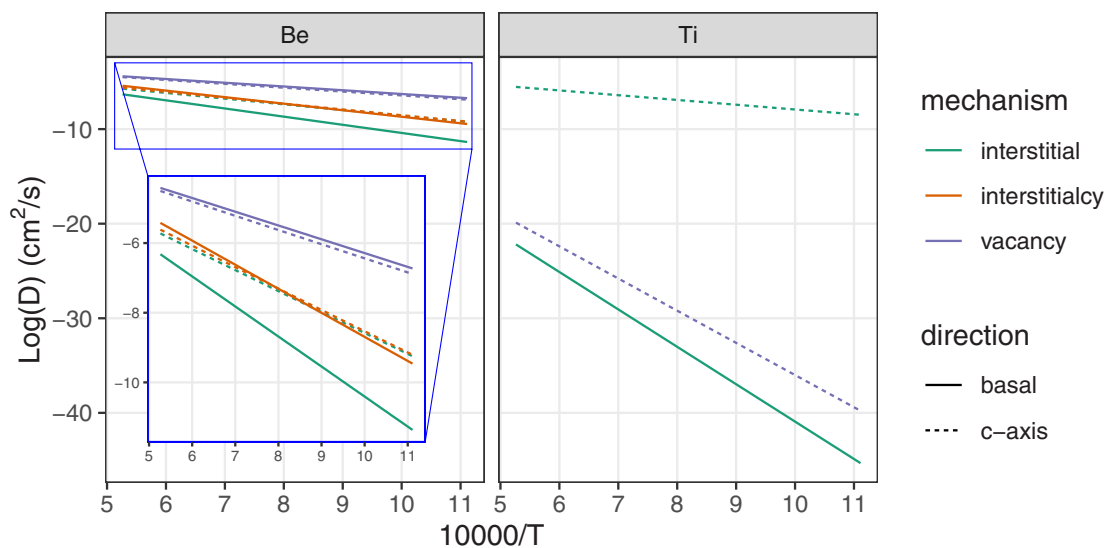


Fig. 5. Arrhenius plots of the concentration-normalised diffusivity of Be and Ti by interstitial, interstitialcy and vacancy mediated mechanisms.

via a vacancy mechanism shows a strong linear correlation between  $x$  and  $E_m$ , while this is not the case for interstitial and interstitialcy mechanisms.

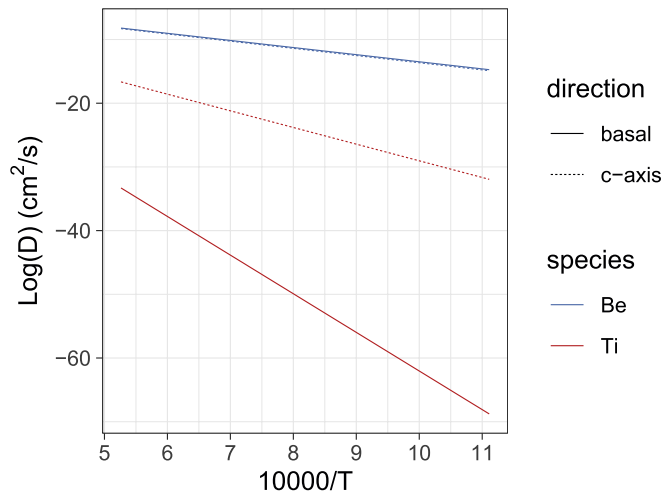
The migration and formation energies were used to predict the self-diffusivity of  $Be_{12}Ti$  using a Green function approach, implemented

within the Onsager code of Trinkle [38,39] (see Fig. 5). The diffusivity of intrinsic species is determined by the mobility of this species, dictated by the activation energy for migration, and the concentration of available defects, dictated by the formation energy of the defects. Thus, in equilibrium conditions, the apparent activation energy for self-diffusion is

**Table 5**

Self-diffusivity coefficients for different species (Be and Ti), different migration mechanisms (interstitial, interstitialcy, and vacancy-mediated) and directions ( $\parallel$  and  $\perp$ ).

	$D_0$ ( $\text{cm}^2\text{s}^{-1}$ )	$E_f$ (eV)	$E_m$ (eV)
$D_{\text{int},\parallel}^{\text{Be}}$	$1.65 \cdot 10^{-2}$	-1.86	-1.71
$D_{\text{int},\perp}^{\text{Be}}$	$0.28 \cdot 10^{-2}$	-1.86	-1.20
$D_{\text{ilcy},\parallel}^{\text{Be}}$	$1.64 \cdot 10^{-2}$	-1.86	-1.37
$D_{\text{ilcy},\perp}^{\text{Be}}$	$0.41 \cdot 10^{-2}$	-1.86	-1.22
$D_{\text{vac},\parallel}^{\text{Be}}$	$0.46 \cdot 10^{-2}$	-1.43	-0.78
$D_{\text{vac},\perp}^{\text{Be}}$	$0.44 \cdot 10^{-2}$	-1.43	-0.81
$D_{\text{vac},\perp}^{\text{Ti}}$	$1.04 \cdot 10^{-2}$	-4.10	-6.75
$D_{\text{int},\parallel}^{\text{Ti}}$	$4.13 \cdot 10^{-2}$	-4.19	-7.85
$D_{\text{int},\perp}^{\text{Ti}}$	$0.13 \cdot 10^{-2}$	-4.19	-1.00

**Fig. 6.** Self-diffusion coefficient of Ti and Be in  $\text{Be}_{12}\text{Ti}$  at thermal equilibrium.

the product of the formation and migration energies. However, when exposed to fast neutron flux, the concentration of defects may be dictated not by thermodynamic equilibrium, but by the rate of formation and recombination of defects from collision cascades. This may lead to

**Table 6**

Lowest energy divacancy hops between single beryllium sites in a beryllium divacancy, and beryllium and titanium sites in a mixed beryllium-titanium divacancy. R is reactant and P is product. In bold the transitions that take part in the lowest energy migration pathway for the  $\text{V}_{\text{Be}}\text{V}_{\text{Be}}$  cluster.

Be-Be divacancy	$E_m$ (eV)		$E_f + E_m$ (eV)	Be-Ti divacancy	$E_m$ (eV)		$E_f + E_m$ (eV)
	from R	from P			from R	from P	
$\text{V}_{\text{Be}2}\text{V}_{\text{Be}3} \rightarrow \text{V}_{\text{Be}2}\text{V}_{\text{Be}1}$	<b>0.48</b>	<b>0.37</b>	<b>3.44</b>	$\text{V}_{\text{Be}2}\text{V}_{\text{Ti}} \rightarrow \text{V}_{\text{Be}1}\text{V}_{\text{Ti}}$	0.95	0.53	6.06
$\text{V}_{\text{Be}2}\text{V}_{\text{Be}2} \rightarrow \text{V}_{\text{Be}2}\text{V}_{\text{Be}3}$ (1)	<b>0.63</b>	<b>0.53</b>	<b>3.56</b>	$\text{V}_{\text{Be}1}\text{V}_{\text{Ti}} \rightarrow \text{V}_{\text{Be}3}\text{V}_{\text{Ti}}$	0.68	0.71	6.19
$\text{V}_{\text{Be}2}\text{V}_{\text{Be}2} \rightarrow \text{V}_{\text{Be}2}\text{V}_{\text{Be}1}$ (2)	<b>0.76</b>	<b>0.70</b>	<b>3.82</b>	$\text{V}_{\text{Be}1}\text{V}_{\text{Ti}} \rightarrow \text{V}_{\text{Be}1}\text{V}_{\text{Ti}}$	1.26	1.26	4.50
$\text{V}_{\text{Be}2}\text{V}_{\text{Be}1} \rightarrow \text{V}_{\text{Be}3}\text{V}_{\text{Be}3}$	0.74	0.53	3.85	$\text{V}_{\text{Be}2}\text{V}_{\text{Ti}} \rightarrow \text{V}_{\text{Be}2}\text{V}_{\text{Ti}}$	0.48	0.48	5.60
$\text{V}_{\text{Be}2}\text{V}_{\text{Be}2} \rightarrow \text{V}_{\text{Be}2}\text{V}_{\text{Be}1}$ (3)	1.08	0.76	3.89	$\text{V}_{\text{Be}2}\text{V}_{\text{Ti}} \rightarrow \text{V}_{\text{Be}3}\text{V}_{\text{Ti}}$	0.83	0.45	5.95
$\text{V}_{\text{Be}2}\text{V}_{\text{Be}2} \rightarrow \text{V}_{\text{Be}2}\text{V}_{\text{Be}1}$ (3)	0.76	0.69	3.89	$\text{V}_{\text{Be}3}\text{V}_{\text{Ti}} \rightarrow \text{V}_{\text{Be}3}\text{V}_{\text{Ti}}$	0.59	0.59	6.08
$\text{V}_{\text{Be}1}\text{V}_{\text{Be}1} \rightarrow \text{V}_{\text{Be}2}\text{V}_{\text{Be}3}$	0.70	0.95	3.90	$\text{V}_{\text{Ti}}$ jumps			
$\text{V}_{\text{Be}2}\text{V}_{\text{Be}2} \rightarrow \text{V}_{\text{Be}2}\text{V}_{\text{Be}2}$ (2)	1.08	0.86	3.92	$\text{V}_{\text{Be}3}\text{V}_{\text{Ti}} \rightarrow \text{V}_{\text{Be}3}\text{V}_{\text{Ti}}$	4.44	4.44	9.93
$\text{V}_{\text{Be}2}\text{V}_{\text{Be}2} \rightarrow \text{V}_{\text{Be}2}\text{V}_{\text{Be}2}$ (2)	1.17	0.77	3.99	$\text{V}_{\text{Be}1}\text{V}_{\text{Ti}} \rightarrow \text{V}_{\text{Be}1}\text{V}_{\text{Ti}}$	6.03	6.03	11.54
$\text{V}_{\text{Be}3}\text{V}_{\text{Be}3} \rightarrow \text{V}_{\text{Be}1}\text{V}_{\text{Be}3}$	0.71	0.77	4.01				
$\text{V}_{\text{Be}2}\text{V}_{\text{Be}2} \rightarrow \text{V}_{\text{Be}2}\text{V}_{\text{Be}3}$ (5)	0.97	1.15	4.05				
$\text{V}_{\text{Be}1}\text{V}_{\text{Be}1} \rightarrow \text{V}_{\text{Be}2}\text{V}_{\text{Be}1}$	0.76	0.99	4.07				
$\text{V}_{\text{Be}2}\text{V}_{\text{Be}2} \rightarrow \text{V}_{\text{Be}2}\text{V}_{\text{Be}3}$ (4)	0.94	1.27	4.10				
$\text{V}_{\text{Be}2}\text{V}_{\text{Be}3} \rightarrow \text{V}_{\text{Be}1}\text{V}_{\text{Be}3}$	0.98	0.64	4.14				
$\text{V}_{\text{Be}3}\text{V}_{\text{Be}3} \rightarrow \text{V}_{\text{Be}2}\text{V}_{\text{Be}3}$	0.9	1.3	4.20				
$\text{V}_{\text{Be}2}\text{V}_{\text{Be}3} \rightarrow \text{V}_{\text{Be}2}\text{V}_{\text{Be}3}$	1.4	1.2	4.34				
$\text{V}_{\text{Be}2}\text{V}_{\text{Be}3} \rightarrow \text{V}_{\text{Be}1}\text{V}_{\text{Be}3}$ (2)	1.2	0.98	4.41				
$\text{V}_{\text{Be}3}\text{V}_{\text{Be}3} \rightarrow \text{V}_{\text{Be}2}\text{V}_{\text{Be}3}$ (2)	3.53	3.82	6.76				
$\text{V}_{\text{Be}2}\text{V}_{\text{Be}2} \rightarrow \text{V}_{\text{Be}2}\text{V}_{\text{Be}2}$ (1)	4.01	3.72	6.82				
$\text{V}_{\text{Be}2}\text{V}_{\text{Be}3} \rightarrow \text{V}_{\text{Be}2}\text{V}_{\text{Be}2}$ (3)	4.58	4.65	7.74				

defect concentration that are orders of magnitude greater than that predicted by thermodynamic equilibrium at the given temperature. In such cases, the formation energy of the defects becomes irrelevant, and it is more appropriate to consider only the migration component of the activation energy. Thus, for convenience, in Fig. 5 we only report the migration component of the diffusivity (i.e. diffusivity normalised by defect concentration), while the self-diffusion coefficient resulting from a thermal equilibrium concentration of defects is presented later.

Fig. 5 shows that Beryllium diffusion is dominated by the vacancy mediated mechanism, which is almost isotropic. Beryllium interstitials migrate 2–5 orders of magnitude more slowly, with the interstitialcy mechanism considerably more favourable than the interstitial only process. Like the vacancy, the interstitialcy mechanism is also close to isotropic. Titanium migration is strongly anisotropic and dominated by the interstitial mechanism, specifically the  $\text{Ti}_{i2} \rightarrow \text{Ti}_{i4}$  transition along the c-axis. In this direction alone, the diffusivity and the activation energy for titanium diffusion is comparable to that of beryllium.

The basal ( $\parallel$ ) and c-axis ( $\perp$ ) diffusion coefficients for each of the species and mechanisms are reported in Table 5. The activation energy has been split between the component due to equilibrium defect concentration (which may be neglected if the defect concentration is dictated by athermal processes), and the migration components, following:

$$D = D_0 \cdot \exp\left(\frac{-(E_f + E_m)}{k_B T}\right) = D_0 \cdot \underbrace{\exp\left(\frac{-E_f}{k_B T}\right)}_{c^{eq}} \cdot \underbrace{\exp\left(\frac{-E_m}{k_B T}\right)}_{\text{migration}}$$

The total diffusivity for a given chemical species (Be or Ti) is given by the sum of the individual contributing diffusion mechanisms. The self-diffusivity was calculated for the case in which intrinsic defect concentrations were dictated by thermal equilibrium, as shown in Fig. 6. It is evident that all Be diffuse isotropically in the range of  $10^{-14}$  –  $10^{-8}$   $\text{cm}^2\text{s}^{-1}$  in the temperature range of 900 K–1400 K, while Ti is virtually sessile at all but the highest temperatures, as expected by the very low equilibrium concentration of Ti defects.

### 3.4. Cluster migration

Previous work [29] showed that several  $\text{V}_{\text{Be}}\text{V}_{\text{Be}}$  and  $\text{V}_{\text{Be}}\text{V}_{\text{Ti}}$  clusters exhibit negative binding energies, thus migration of these stable species must also be considered. This is challenging given the large number of

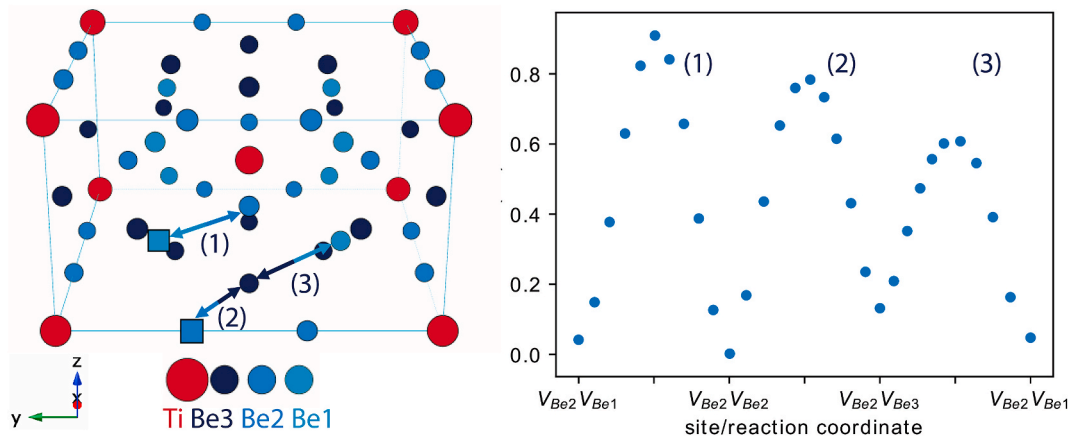


Fig. 7. Lowest migration energy contiguous migration pathway between beryllium divacancies predicted using the NEB methodology.

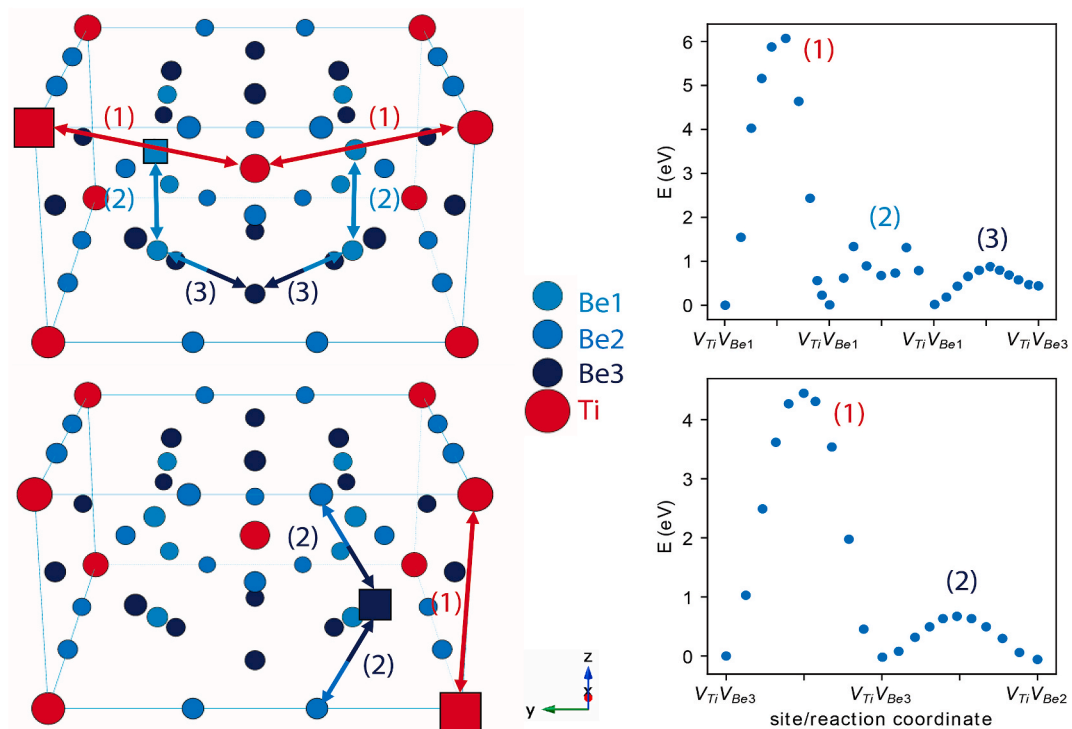


Fig. 8. Lowest migration energy contiguous migration pathways for the mixed beryllium titanium divacancies in (top) the [111] direction and (bottom) [001] direction.

possible starting configurations: for  $V_{Be}V_{Be}$  species, there are 9 unique nearest neighbour configurations and 72 nearest neighbour transitions (where a single vacancy is exchanged, for example,  $V_{Be2}V_{Be2} \rightarrow V_{Be2}V_{Be1}$ ). Using symmetry considerations this number can be reduced to 21 possible transitions [29]. Migration energies for these transitions, along with those of  $V_{Be}V_{Ti}$ , calculated using combined LST-QST calculations, are presented in Table 6.

The lowest energy contiguous migration pathway for beryllium divacancies is via the  $V_{Be2}V_{Be1} \rightarrow V_{Be2}V_{Be2} \rightarrow V_{Be2}V_{Be3} \rightarrow V_{Be2}V_{Be1}$  pathway, with migration energies of 0.76, 0.63 and 0.48 eV respectively (although there are many other transitions with similar migration energy). The calculated NEB pathway for this migration route is shown in Fig. 7. The rate limiting process  $V_{Be2}V_{Be2} \rightarrow V_{Be2}V_{Be3}$  has energy 0.76 eV, which is the same as that for isolated vacancy diffusion, thus this pathway is not expected to substantially alter the temperature dependence of vacancy diffusion in this material, except that this divacancy

pathway is isotropic.

The mechanism for mixed  $V_{Be}V_{Ti}$  migration is comprised of two steps:

- i) migration of the  $V_{Ti}$  species from one site to another (bridged by the  $V_{Be}$  species), and
- ii) reorientation of the  $V_{Be}$  species around the larger  $V_{Ti}$  species.

The first step, in all cases, has significantly higher migration energy (i.e. it is rate determining), with 6.03 eV in the [111] direction ( $V_{Ti(000)}V_{Be1} \rightarrow V_{Ti(0.5,0.5,0.5)}V_{Be1}$ ) and 4.44 eV in the [001] direction ( $V_{Ti(000)}V_{Be3} \rightarrow V_{Ti(111)}V_{Be3}$ ), which means migration of this species is strongly anisotropic favouring the [001] direction.

For Ti diffusion to proceed, the  $V_{Be2}$  species must then re-orientate around the  $V_{Ti}$  species (i.e. the second step). For migration in [111], this requires two unique steps, whereby a transition occurs from  $V_{Ti}V_{Be1}$

(0.25,0.25,0.25) to  $V_{Ti}V_{Be1(0.25,0.25,0.75)}$  with migration energy 1.26 eV (which by itself would facilitate migration in the [001] direction) and a further transition from  $V_{Ti}V_{Be1}$  to  $V_{Ti}V_{Be3}$  with migration energy 0.71 eV. Migration in [001] by the latter  $V_{Ti}$  transition further requires the transition  $V_{Ti}V_{Be3} \rightarrow V_{Ti}V_{Be2}$  with migration energy 0.83 eV. The NEB pathway for isotropic and anisotropic diffusion are shown in Fig. 8. Interestingly, for the isotropic pathway, it appears from the NEB energies that there is a metastable state between the two  $V_{Ti}V_{Be1}$  species.

#### 4. Conclusions

Defect migration processes have been predicted in  $Be_{12}Ti$  using density functional theory in conjunction with the linear/quadratic synchronous transit and nudged elastic band methodology. The choice of which defect processes to focus upon was based on our previous work that identified which single beryllium and titanium vacancies/interstitials were energetically favoured, as well as which small vacancy clusters were stable [29]. Defect formation energies and migration energies were used to predict self-diffusion coefficients for single defect processes using Onsager theory.

It was found that for vacancy-mediated processes, titanium exhibits a much higher migration energy than beryllium. Further, it is predicted that beryllium vacancy migration is only weakly anisotropic with energies of 0.76 eV in the [001] direction and 0.91 eV in the [111] direction. When beryllium di-vacancy clusters are considered even the small anisotropy is removed with di-vacancy mediated transport occurring isotropically with an activation energy of 0.76 eV. Conversely, the only viable titanium vacancy migration pathway occurs in the [001] direction with migration energy 6.75 eV. Even when  $V_{Ti}V_{Be}$  divacancies are considered the activation energy is only reduced to 4.44 eV in [001] although there is now also a mechanism in [111] directions with an activation energy of 6.03 eV.

Diffusion of beryllium interstitial species is also predicted to be close to isotropic, however, transport involving an interstitialcy step is favoured over interstitial only. Conversely, titanium interstitial migration is strongly anisotropic, with migration energy 1.00 eV in the [001] direction while the next lowest energy transition, which facilitates transport isotropically has an energy of 6.92 eV.

These results, especially the stark differences between titanium and beryllium transport, will impact on the formation of extended defects, such as interstitial loops and voids, and by extension the evolution of the thermophysical properties of the material under irradiation.

#### CRedit authorship contribution statement

**M.L. Jackson:** Investigation, Writing - original draft. **P.A. Burr:** Methodology, Writing - review & editing. **R.W. Grimes:** Conceptualization, Resources, Writing - review & editing, Supervision.

#### Declaration of competing interest

The authors declare that they have no known competing financial interests or personal relationships that could have appeared to influence the work reported in this paper.

#### Acknowledgements

MLJ received funding via CCFE from the Euratom research and training programme 2014–2018 under grant agreement No 633053 (EUROfusion Consortium) - the views and opinions expressed herein do not necessarily reflect those of the European Commission. Computing resources were provided by the Imperial College London High Performance Computing Service.

#### Appendix A. Supplementary data

Supplementary data to this article can be found online at <https://doi.org/10.1016/j.intermet.2020.106937>.

#### References

- [1] P. Kurinsky, V. Chakin, A. Moeslang, R. Rolli, E. Alves, L.C. Alves, N. Franco, C. Dorn, A.A. Goraieb, Comparative study of fusion relevant properties of Be12V and Be12Ti, *Fusion Eng. Des.* 86 (2011) 2454–2457.
- [2] J. Reimann, P. Kurinsky, R. Lindau, A. Moeslang, M. Rohde, C. Dorn, W. Haws, A. Goraieb, H. Harsch, C. Linsmeier, Beryllides for fusion reactors, in: 23rd IEEE/NPSS Symposium On Fusion Engineering, IEEE, 2009, pp. 1–4.
- [3] M. Nakamichi, J.H. Kim, P. Kurinsky, M. Nakamura, Thermal properties of beryllides as advanced neutron multipliers for DEMO fusion application, *Nucl. Mater. Energy* 15 (2018) 71–75.
- [4] P. Pereslavtsev, F.A. Hernández, G. Zhou, L. Lu, C. Wegmann, U. Fischer, Nuclear analyses of solid breeder blanket options for DEMO: status, challenges and outlook, *Fusion Eng. Des.* 146 (2019) 563–567.
- [5] F.A. Hernández, P. Pereslavtsev, G. Zhou, B. Kiss, Q. Kang, H. Neuberger, V. Chakin, R. Gaisin, P. Vladimirov, L.V. Bocaccini, G.A. Spagnuolo, S. D'Amico, I. Moscato, Advancements in the helium-cooled pebble bed breeding blanket for the EU DEMO: holistic design approach and lessons learned, *Fusion Sci. Technol.* 75 (2019) 352–364.
- [6] J.-H. Kim, M. Nakamichi, Fabrication and characterization of crushed titanium–beryllium intermetallic compounds, *J. Nucl. Mater.* 498 (2018) 249–253.
- [7] R. Gaisin, V. Chakin, R. Rolli, J. Hoffmann, H. Leiste, T. Bergfeldt, U. Jäntschi, M. Klimentov, J. Lorenz, A. Goraieb, P. Vladimirov, A. Möslang, Synthesis of Be12Ti compound via arc melting or hot isostatic pressing, *J. Alloys Compd* (2019), 152919.
- [8] V. Chakin, M. Klimentov, R. Rolli, P. Kurinsky, A. Moeslang, C. Dorn, Microstructural and tritium release examination of titanium beryllides, *J. Nucl. Mater.* 417 (2011) 769–774.
- [9] V. Chakin, R. Rolli, A. Moeslang, P. Kurinsky, Tritium and helium release from highly neutron irradiated titanium beryllide, *Fusion Eng. Des.* (2015), <https://doi.org/10.1016/j.fusengdes.2015.01.038>.
- [10] A.V. Fedorov, S. Van Til, M.P. Stijkel, M. Nakamichi, M. Zmitko, Post irradiation characterization of beryllium and beryllides after high temperature irradiation up to 3000 appm helium production in HIDOBE-01, *Fusion Eng. Des.* 102 (2016) 74–80.
- [11] X. Zhao, M. Ni, B. Nie, B. Zhang, L. Chen, K. Huang, S. Liu, 3D tritium transport analysis for WCCB blanket based on COMSOL, *Fusion Eng. Des.* 151 (2020) 111405.
- [12] V. Chakin, R. Rolli, R. Gaisin, P. Kurinsky, J.-H. Kim, M. Nakamichi, Effect of heat treatment of titanium beryllide on tritium/hydrogen release, *Fusion Eng. Des.* 137 (2018) 165–171.
- [13] J.-H. Kim, M. Nakamichi, Fabrication and characterization of Be-Zr-Ti ternary beryllide pebbles, *Fusion Eng. Des.* 136 (2018) 864–868.
- [14] O. Neubauer, R. Koch, P. Mertens, T. Verhoeven, P. Kurinsky, A. Moeslang, V. Chakin, M. Klimentov, R. Rolli, S. van Til, A.A. Goraieb, Characteristics of microstructure, swelling and mechanical behaviour of titanium beryllide samples after high-dose neutron irradiation at 740 and 873K, *Fusion Eng. Des.* 88 (2013) 2198–2201.
- [15] P. Kurinsky, R. Rolli, J.H. Kim, M. Nakamichi, Mechanical behavior of Be-Ti pebbles at blanket relevant temperatures, *Fusion Eng. Des.* 109 (2015) 764–767.
- [16] H. Yamada, Y. Nagao, H. Kawamura, M. Nakao, M. Uchida, H. Ito, Preliminary neutronic estimation for demo blanket with beryllide, *Fusion Eng. Des.* 69 (2003) 269–273.
- [17] S.C. Middleburgh, R.W. Grimes, Defects and transport processes in beryllium, *Acta Mater.* 59 (2011) 7095–7103.
- [18] W.H. Robbins, H.B. Finger, An historical perspective of the NERVA nuclear rocket engine technology program, 1991, <https://doi.org/10.2514/6.1991-3451>.
- [19] R.J.M. Konings, T.R. Allen, R.E. Stoller, S. Yamanaka, *Comprehensive Nuclear Materials*. (Elsevier Ltd., Amsterdam, Netherlands., 2012).
- [20] M.E. Kolanz, Introduction to beryllium: uses, regulatory history, and disease, *Appl. Occup. Environ. Hyg* 16 (2001) 559–567.
- [21] P. Kurinsky, H. Leiste, A. Goraieb, R. Rolli, S. Mueller, J. Reimann, A. Moeslang, Production of Be-Ti and Be-Zr rods by extrusion and their characterization, *Fusion Eng. Des.* 136 (2018) 49–52.
- [22] M. Uchida, E. Ishitsuka, H. Kawamura, Thermal conductivity of neutron irradiated Be12Ti, *Fusion Eng. Des.* 69 (2003) 499–503.
- [23] M. Uchida, E. Ishitsuka, H. Kawamura, Tritium release properties of neutron-irradiated Be12Ti, *J. Nucl. Mater.* 307–311 (2002) 653–656.
- [24] A. Allouche, N. Fernandez, Y. Ferro, Hydrogen retention and diffusion in tungsten beryllide, *J. physics. Condens. matter* 26 (2014) 315–322.
- [25] Y. Fujii, M. Miyamoto, J.-H. Kim, M. Nakamichi, N. Murayoshi, H. Iwakiri, Hydrogen retention behavior of beryllides as advanced neutron multipliers, *Nucl. Mater. Energy* 9 (2015) 233–236.
- [26] X. Zhu, C. Wang, Z. Meng, Y. Wang, H. Deng, W. Duan, L. Yang, First-principles study of hydrogen-vacancy complexes in Be12Ti, *J. Nucl. Mater.* 525 (2019) 7–13.
- [27] X. Zhu, C. Wang, J. Liu, X. Zhang, H. Deng, W. Duan, L. Yang, Retention and diffusion of transmutation H and He atoms in Be<sub>12</sub>Ti: first-principles calculations, *RSC Adv.* 8 (2018) 35735–35743.

- [28] D.V. Bachurin, P.V. Vladimirov, Ab initio study of Be and Be<sub>12</sub>Ti for fusion applications, *Intermetallics* 100 (2018) 163–170.
- [29] M.L. Jackson, P.A. Burr, R.W. Grimes, Defect processes in Be<sub>12</sub>X (X = Ti, Mo, V, W), *Nucl. Fusion* 57 (2017) 86049.
- [30] J.P. Perdew, K. Burke, M. Ernzerhof, Generalized gradient approximation made simple, *Phys. Rev. Lett.* 77 (1996) 3865–3868.
- [31] M.D. Segall, P.J.D. Lindan, M.J. Probert, C.J. Pickard, P.J. Hasnip, S.J. Clark, M. C. Payne, First-principles simulation: ideas, illustrations and the CASTEP code, *J. Phys. Condens. Matter* 14 (2002) 2717–2744.
- [32] H.J. Monkhorst, J.D. Pack, Special points for Brillouin-zone integrations, *Phys. Rev. B* 13 (1976) 5188–5192.
- [33] M. Methfessel, A. Paxton, High-precision sampling for Brillouin-zone integration in metals, *Phys. Rev. B* 40 (1989) 3616–3621.
- [34] T.A. Halgren, W.N. Lipscomb, The synchronous-transit method for determining reaction pathways and locating molecular transition states, *Chem. Phys. Lett.* 49 (1977) 225–232.
- [35] N. Govind, M. Petersen, G. Fitzgerald, D. King-Smith, J. Andzelm, A generalized synchronous transit method for transition state location. in, *Comput. Mater. Sci.* 28 (2003) 250–258.
- [36] H. Jónsson, G. Mills, K.W. Jacobsen, Nudged elastic band method for finding minimum energy paths of transitions. in 385–404, World Scientific Pub Co Pte Lt, 1998.
- [37] H. Mehrer, *Diffusion in Solids: Fundamentals, Methods, Materials, Diffusion-Controlled Processes*, Springer, 2007.
- [38] D.R. Trinkle, Diffusivity and derivatives for interstitial solutes: activation energy, volume, and elastodiffusion tensors, *Philos. Mag. A* 96 (2016) 2714–2735.
- [39] D.R. Trinkle, Automatic numerical evaluation of vacancy-mediated transport for arbitrary crystals: Onsager coefficients in the dilute limit using a Green function approach, *Philos. Mag. A* 97 (2017) 2514–2563.
- [40] M. Nastar, A mean field theory for diffusion in a dilute multi-component alloy: a new model for the effect of solutes on self-diffusion, *Philos. Mag. A* 85 (2005) 3767–3794.
- [41] M. Nastar, Atomic diffusion theory challenging the Cahn-Hilliard method, *Phys. Rev. B Condens. Matter* 90 (2014) 144101.
- [42] T. Schuler, L. Messina, M. Nastar, KineCluE: a kinetic cluster expansion code to compute transport coefficients beyond the dilute limit, *Comput. Mater. Sci.* 172 (2020) 109191.
- [43] M.L. Jackson, *Atomistic Simulations of Materials for Nuclear Fusion*, Imperial College London, 2018.
- [44] P.A.A. Burr, S.X.X. Oliver, Formation and migration of point defects in tungsten carbide: unveiling the sluggish bulk self-diffusivity of WC, *J. Eur. Ceram. Soc.* 39 (2018) 165–172.
- [45] P.A. Burr, E. Kardoulaki, R. Holmes, S.C. Middleburgh, Defect evolution in burnable absorber candidate material: uranium diboride, UB<sub>2</sub>, *J. Nucl. Mater.* 513 (2019) 45–55.
- [46] A. Zalkin, D.E. Sands, R.G. Bedford, O.H. Krikorian, The beryllides of Ti, V, Cr, Zr, Nb, Mo, Hf and Ta, *Acta Crystallogr.* 14 (1961) 63–65.
- [47] M.L. Jackson, P.A. Burr, R.W. Grimes, Resolving the structure of TiBe<sub>12</sub>, *Acta Crystallogr. Sect. B Struct. Sci. Cryst. Eng. Mater.* 72 (2016) 277–280.
- [48] X. Liu, Q. Feng, B. Tang, J. Zheng, Z. Zheng, W. Zhou, J. Tian, J. Wang, First-principles calculations of mechanical and thermodynamic properties of tetragonal Be<sub>12</sub>Ti, *RSC Adv.* 9 (2019) 5302–5312.